In-situ Calibration of Four-Hole Pressure Probes on a Small UAV for Free Flight Measurement

Jürgen Frey[1], David Nölle[2] and Harald Pfifer[3]
Technische Universität Dresden, 01307 Dresden, Germany

Daniel Ossmann[4]
Munich University of Applied Sciences HM, 08335, Munich, Germany

This paper describes the calibration process of cone-shaped four-hole pressure probes to be used for wind estimation based on airborne sensing with small unmanned aerial vehicles (UAVs). Due to the limited payload capacity and system resources of small UAVs, the probes do only have four holes in contrast to conventional five-hole probes. The probes are calibrated solely and together with the aircraft in a wind tunnel to cover retroactive effects originating from the flow field around the airframe. A lifting line model is set up to accompany this approach and to correct test section blockage. The calibration is approximated by polynomial functions of fifth and fourth order for main and cross sensitivities, respectively. The fitting results show a satisfactory representation of the probes' behavior within the calibrated range of flow angles, that covers the expected flight envelope very well. As a result, four-hole probes can be called applicable for the task of flow angle measurement at small UAVs.

I. Nomenclature

$A_{i,j}$	=	calibration coefficient for a pneumatic probe's angle of attack
$B_{i,j}$	=	calibration coefficient for a pneumatic probe's yawing angle
c_L	=	lift coefficient
c_p	=	pressure coefficient
c	=	chord length
K_i	=	polynomial fitting parameter of airfoil thickness effect on flow angle
p	=	pressure
p_i	=	pressure measured at port i of a pneumatic probe
p_{REF}	=	reference pressure for calibration functions of pneumatic probes
q	=	dynamic pressure
q_∞	=	free stream dynamic pressure
$Q_{i,j}$	=	calibration coefficient for the dynamic pressure measured by a pneumatic probe
u	=	flow velocity, velocity component in x-direction
X	=	argument for calibration function representing angle of attack
Y	=	argument for calibration function representing angle of sideslip
α	=	angle of attack
α_{EFF}	=	effective angle of attack

[1] Research Assistant, Chair of Flight Mechanics and Control, juergen.frey@tu-dresden.de
[2] Research Assistant, Chair of Flight Mechanics and Control, david.noelle@tu-dresden.de
[3] Professor, Chair of Flight Mechanics and Control, harald.pfifer@tu-dresden.de
[4] Professor, Department of Mechanical, Automotive and Aeronautical Engineering, daniel.ossmann@hm.edu, AIAA Senior Member

β = angle of sideslip
φ = roll angle
θ = yaw angle

AoA = angle of attack
AoS = angle of sideslip
GPS = global positioning system
IMU = inertial measurement unit
LES = large eddy simulation
UAV = unmanned aerial vehicle

II. Introduction

Unmanned aerial vehicles (UAVs) are used for a rapidly growing variety of tasks, including the assessment of large technical facilities, the monitoring of infrastructure or detailed terrain surveillance. Typically, UAVs are very small, light aircraft operating at low airspeeds that show great sensitivity to the atmospheric wind. Particularly in the case of battery-electric UAVs, range and endurance are rather limited by the low energy density. These two performance parameters can be improved by taking advantage of the wind sensitivity and flying in favorable conditions that are tailwind and upwind. For fixed-wing UAV, the latter one is the more effective [1].

For optimal flight path planning, the local wind and weather data are the most crucial parameters and must be made available or predictable. Within previous work, these data were gathered numerically from Large Eddy Simulations (LES) [1] and wind tunnel measurements [2]. Particularly the wind tunnel experiments revealed a highly unsteady local wind field that can hardly be predicted from regional wind data provided by stationary weather sensors. To improve the knowledge on local wind situations, the research described in this paper is focused on the determination of real-world wind data using airborne sensing.

Basically, the wind vector is the difference between the UAV's movement in space and in its surrounding air mass. The velocity vector in space can be determined from an inertial measurement unit (IMU), that is typically augmented by data from a global positioning system (GPS). The relative flow can either be estimated from the control and power setting of the UAV [3], or measured using a suitable kind of anemometer [4, 5]. The first approach requires adequate knowledge about the UAV's aerodynamic properties. In the latter case, the airframe' effect on the local flow field has to be accounted for.

As the relevance of this topic continues to increase, a lot of research is currently taking place upon wind field measurement with UAVs. Recent research, however, mainly focuses on multicopters [3, 4, 5]. Fixed-wing UAVs play a minor role so far, even though they provide better range and endurance as a matter of principle. For this reason, fixed-wing UAVs are the focus of this paper.

As a fixed-wing aircraft experiences only a limited range of flow angles in controlled flight, the flow vector can reliably be measured using multi-hole pressure probes. The standard case is the five-hole probe with a pyramidal or conical head [6]. A larger number of holes usually results in an increased range of flow angles that can be covered, but also requires a larger number of pressure transducers and sampling channels [7]. In contrast, probes with fewer holes are justified for smaller flow angle ranges. They also offer the advantage of a smaller probe size and a minimum of consecutive measurement technology, which is especially beneficial for small UAVs with limited payload capacity. In the case presented here, cone-shaped probes with only four holes have been used for the purpose of flow measurement on a small UAV.

Shepherd [8] described a pyramid-shaped four-hole probe and its calibration in 1981. In the meantime, commercial suppliers such as Turbulent Flow Instrumentation (TFI) provide such probes of the shelf [9]. The feasibility of four-hole pressure probes on multicopter UAVs has been studied before [4]. A cone-shaped four-hole probe was used in house for free flight measurement before and showed adequate properties [10].

Within the scope of the work presented in this publication, two cone-shaped probes are installed on a small UAV (one under each wing) to measure the local flow vector with respect to the airframe. By subtracting this vector from the inertial velocity vector in space, the wind field can be estimated and fed into an algorithm for flight path optimization. This paper is focused in the part concerning the pressure probes (Section III.) and their calibration in the wind tunnel (Section IV.). This is done solo as well as in situ with the UAV that will carry these probes in free flight. In the latter case, the local flow field imposed to the probe head by the airframe is part of the calibration data. The calibration procedure is subject of Section IV.B. and IV.C. Further corrections have to be applied only for upstream

effects originating from deflected control surfaces and the angular motion of the aircraft that imposes additional velocities to the probe heads. Accompanying lifting-line calculations are intended to estimate the differences to be expected between solo and in-situ calibration (Section IV.A.). The final Section V. presents relevant result, especially concerning the quality of the fitting functions, in how far they are able to represent the calibration data. Moreover, the measurement data are compared to the lifting line results concerning the upstream influence of the entire airframe, flap and aileron deflection as well as rolling and pitching motion.

III. Experimental Test Setup

The test setup consists of the fixed-wing UAV *UrbanCondor* that carries the cone-shaped pressure probes with four holes intended for flow measurement in free flight. The main test facility is the low-speed wind tunnel in Dresden. The test aircraft as well as the wind tunnel itself are briefly described in the following Section. Subsection III.C. describes the cone-shaped four-hole probe and the mathematical formulation of its calibration.

A. UAV *UrbanCondor*

The UAV used is a SIG Kadet LT-40 [11] with a modified wing, called *UrbanCondor* (Fig. 1). This wing has an increased span (2 m compared to 1.78 m) and flaps, allowing a higher take-off weight and payloads up to 2 kg. The spar is a continuous carbon-fiber square tube with a number of 3D-printed elements threaded onto it. This way, damaged components can be replaced more easily. Due to the end-to-end spar, the *Urban Condor* has no dihedral. Still, pilot statements confirm satisfactory handling qualities for the aircraft after several piloted flight tests.

The two pressure probes are mounted under the wing at half span on both sides, determining the flight attitude with respect to the surrounding air mass by measuring pressures acting on the probe. Using two probes provides redundancy and the possibility to determine the roll rate. Other components, such as motor, propeller, accumulator and control system, are commercial of the shelf products.

Fig. 1 UAV *UrbanCondor* carrying a payload mockup during its maiden flight.

B. Low-Speed Wind Tunnel at TU Dresden

The Chair of Flight Mechanics and Control at TU Dresden operates a low-speed Göttingen-type wind tunnel with a closed circuit and an open test section, as depicted in Fig. 2. The tunnel has a circular nozzle with a 3-meter diameter and provides flow velocities up to 40 m/s. Its contraction ratio is 7:1, leading to a free stream turbulence below 0.5%, which makes it suitable for aeronautical applications.

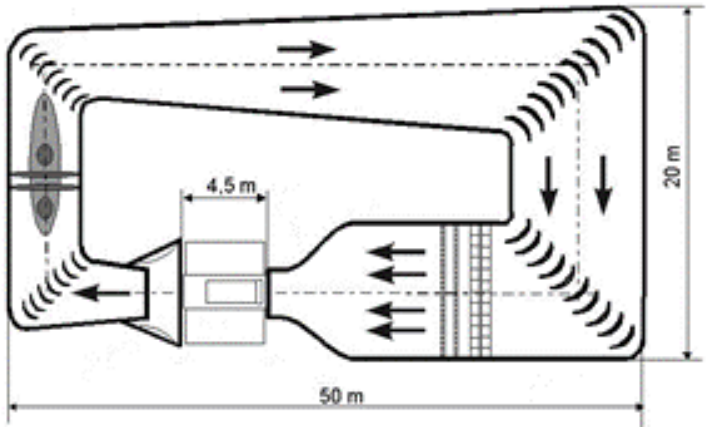

Fig. 2 Schematic of TU Dresden's wind tunnel.

The UAV is fixed within the test section on a sting mounting. The mounting strut is placed on an angular traverse in the floor that allows yaw angle changes. The aircraft is connected to the strut via another angular traverse, allowing changes in rolling angle as shown in the left picture of Fig. 3. For solo calibration, single probes were mounted on a yawing-pitching traverse as depicted in the right image of Fig. 3. This way, angles of attack and sideslip were commanded directly.

Fig. 3 UAV *UrbanCondor* (left) and pressure probe (right) mounted in the test section.

C. Cone-shaped Four-hole Pressure Probes

For application on small UAVs, the number of pressure transducers and sampling channels as well as the size of the probes is an issue due to weight and space constraints. Therefore, a particularly sparing solution is desired: The flow vector is described by its three components, the angle of attack (AoA) - α, the angle of sideslip (AoS) - β, and absolute air velocity u. Thus, only three differential pressures are necessary for its determination, meanwhile standard five-hole probes require four differential pressures at least. Reducing the number of pressure ports to four, a central (total-pressure) hole and three more holes arranged in a 120-degree-angle to each other, results in the smallest probe head possible for the given task. The cone shaped probe used in the presented case are depicted in Fig. 4. Moreover, aircraft including small UAVs usually experience comparatively small changes in AoA and AoS, further justifying the use of probes with the minimum number of holes.

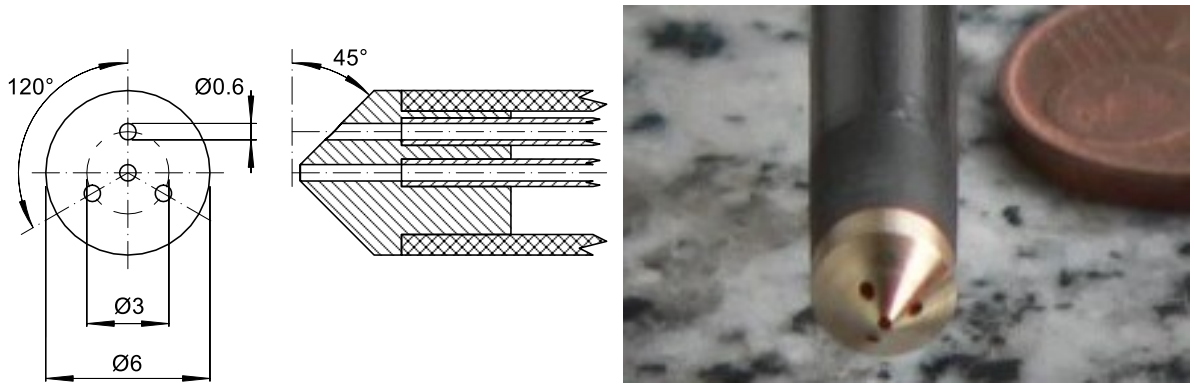

Fig. 4 Schematic view (left) and photograph (right) of a cone-shaped four-hole pressure probe.

The kind of pressure probe described here has been already used for determination of flight attitude on a Let L-23 Super-Blanik in free flight experiments. The probe proved to cover a sufficient range of flow angles. The test yielded to a reasonable lift curve which after correction corresponds well with the lift slope predicted by theory, as shown in Fig. 5 [10]. Moreover, Fig. 5 impressively illustrates the presence of unsteady conditions in free flight. The lift curve was produced with a heavier manned aircraft (compared to UAVs) during the early morning in very calm air and each data point is an average over one second.

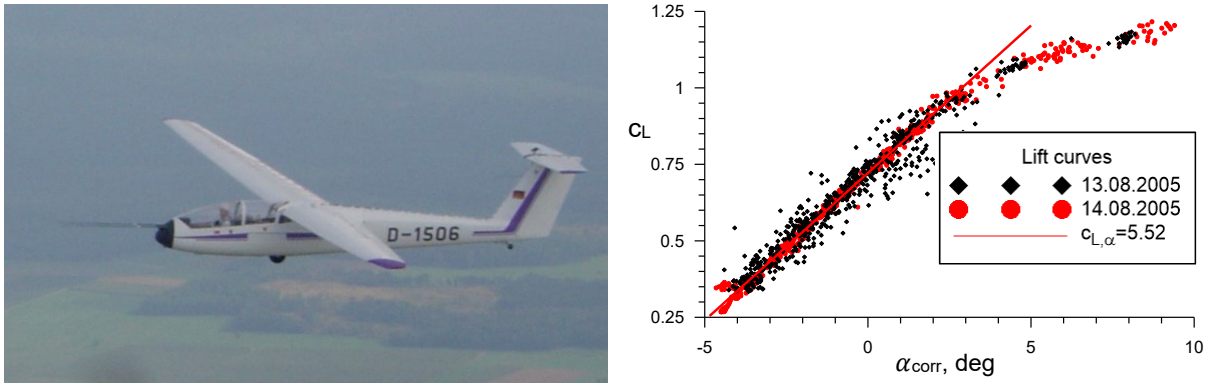

Fig. 5 Let L-23 Super Blanik with nose boom and four-hole probe for measurement of flight attitude (left), lift curves gained from these free flight measurements (right) [10].

Unlike the zonal approach given by Shepherd [8], continuous calibration functions are used in this paper, similar to the approach for five-hole probes given by Treaster and Yocum [6]. This kind of approach has been used successfully for several types of probes before. Since this choice is legitimate for the relatively small angle range, a minimum of computational effort is achieved. When using small UAVs for real-time free-flight measurement, on-board computing performance is still rather limited. Polynomial fitting functions are used to formulate the dependency of the flow vector from the pressure differences between the holes. These pressure differences are represented by the two scalar values X and Y as well as a reference pressure p_{REF}.

$$\alpha = \sum_{i=0}^{5} \sum_{j=0}^{4} A_{i,j} X^i Y^j \tag{1}$$

$$\beta = \sum_{i=0}^{5} \sum_{j=0}^{4} B_{i,j} Y^i X^j \tag{2}$$

$$q = p_{REF} \sum_{i=0}^{4} \sum_{j=0}^{4} Q_{i,j} Y^i X^j \tag{3}$$

where A, B, and Q are the coefficient matrices which are fitted in the calibration. If a pressure probe has only four holes, these holes cannot be arranged in planes perpendicular to each other. Therefore, the formulation of X, Y and p_{REF} is given by:

$$p_{REF} = 3p_1 - p_2 - p_3 - p_4 \tag{4}$$

$$X = \frac{2p_2 - p_3 - p_4}{p_{REF}};\ Y = \frac{p_3 - p_4}{p_{REF}} \tag{5}$$

where p_1 is the pressure reading from the central port (total pressure), p_2 from the upper, p_3 from the left and p_4 from the right port. Note that this formulation of X, Y and p_{REF} differs from the standard used for five-hole probes, as described by Treaster and Yocum [6].

IV. Probe Calibration Procedure

Despite the long nose boom and double-seater cockpit, the flow field upstream of the Blanik's wing required a correction of flow angle changes by 10% [10]. This kind of correction is usually derived from lifting line models, because the influence of lifting vortex systems reaches much farther into the flow field than the displacement of the bodies' thickness. Having a wind tunnel that allows full size measurements on UAVs, calibration is conducted in situ. Doing so, all influences originating from the flow around the aircraft can be taken into account the best way possible.

The calibration of the probes is executed in two steps: At first, the sole probes are calibrated in an undisturbed wind tunnel flow. Afterwards, the local flow field is considered that is imposed by the airframe the probes are attached to. Lifting line calculations are carried out to estimate the differences to be expected between the two procedures as well as to correct test section blockage in the wind tunnel.

A. Lifting Line Model and Estimation of Displacement Caused by Airfoil Thickness

A vortex lattice model of the *UrbanCondor* has been set up within the aerodynamics calculation code Athena Vortex Lattice (AVL) [12]. The lifting line model is visualized in Fig. 6. Using this model, the deformation of the local flow field caused by the aircraft itself can be estimated, including the upstream effects of ailerons and flaps.

Since AVL does not allow to extract flow properties at arbitrary points in the flow field, additional wings have been added to the model at the probe positions. To avoid an influence on the aircraft's properties, these wings have very small chord length resulting in an extremely high aspect ratio of 6000. From the lift coefficient of these tiny wings, the local flow angle can then be obtained. According to the character of the lifting line theory, all effects are completely linear and can be superimposed, even flap and aileron deflections, as depicted in Fig. 7. Meanwhile the upstream effect of the elevator is fairly neglectable, those of aileron and flaps, however, are clearly visible and have to be accounted for.

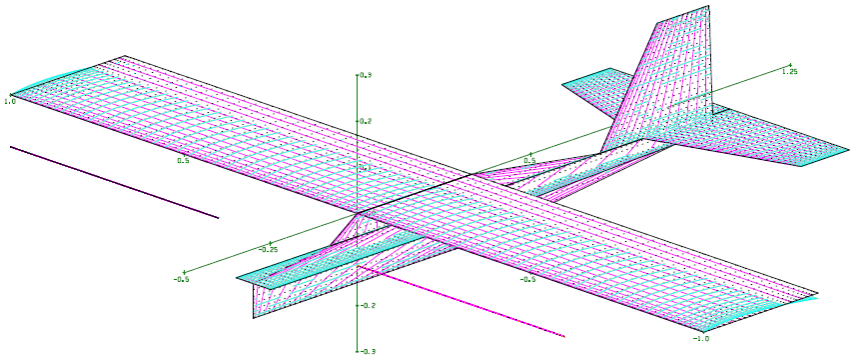

Fig. 6 Lifting line model used in AVL, note the two thin wing segments that represent the probe positions.

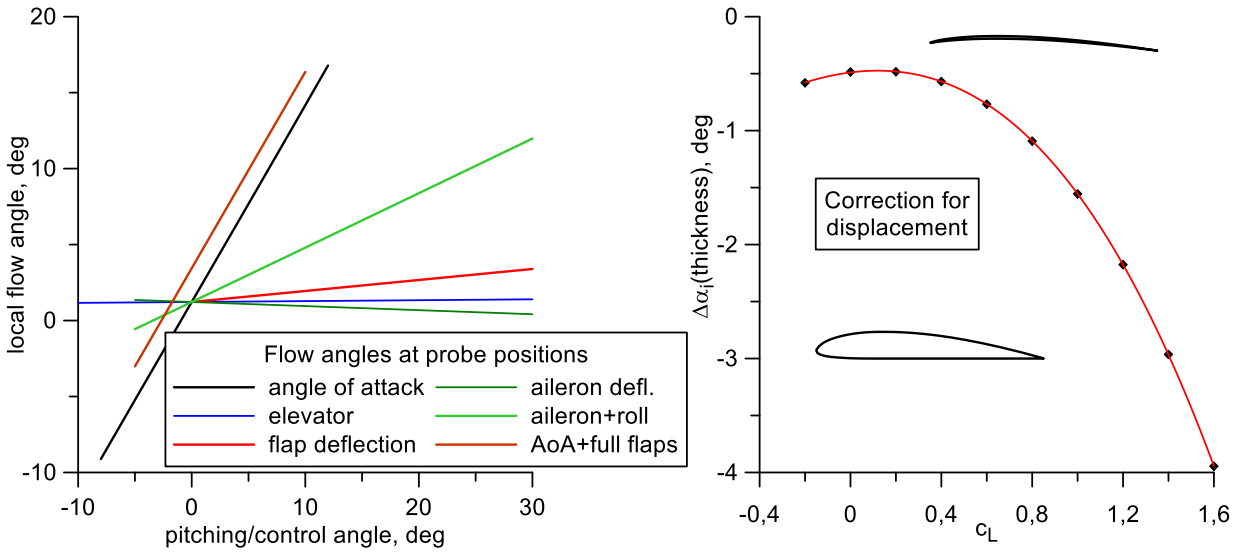

Fig. 7 Expected angle of attack at a probe head depending on aircraft angle of attack, control surface deflection and rolling motion (left), additional flow angle imposed by the displacement of the airfoil's thickness.

Moreover, the displacement caused by the sheer thickness of the airfoil leads to a further deflection of the flow that is not covered by the vortex lattice model in AVL. In order to quantify this effect, flow angles at the probe positions were calculated using the 2D airfoil design tool XFOIL [13]. In order to separate the displacement from the chordwise circulation distribution, the Clark Y airfoil was compared to an airfoil representing almost only its camber line. The difference between both versus the lift coefficient can be fitted by a third-degree polynomial function as shown in the right diagram of Fig. 7. In Eq. (6), α_{ind} represents the induced AoA and K_i the polynomial parameters:

$$\alpha_{ind} = \sum_{i=0}^{3} K_i c_L^i \tag{6}$$

B. Probe Calibration in Undisturbed Flow

The local flow angles at the probe heads are not only influenced by the angles of attack and sideslip. As established in Section IV.A, there are also upstream effects of aileron and flap deflection as well as the aircraft's rolling, pitching and yawing motion. Thus, calibrating all these factors in one shot would require uneconomically high effort. Therefore, a calibration of the probes without aircraft is performed first.

The calibration was carried out for pitch and yaw angles reaching from -10 deg to $+10$ deg. for the first probe. For probe 2, the pitch angle range has been increased to ± 20 deg in order to check the validity range of the probes. The free stream velocity was set to 15 m/s for all calibration cases. Within the given range of flow angles, the fitting functions can reproduce the behavior of the probe very well, as the recalculated angles depicted in Fig. 8 indicate.

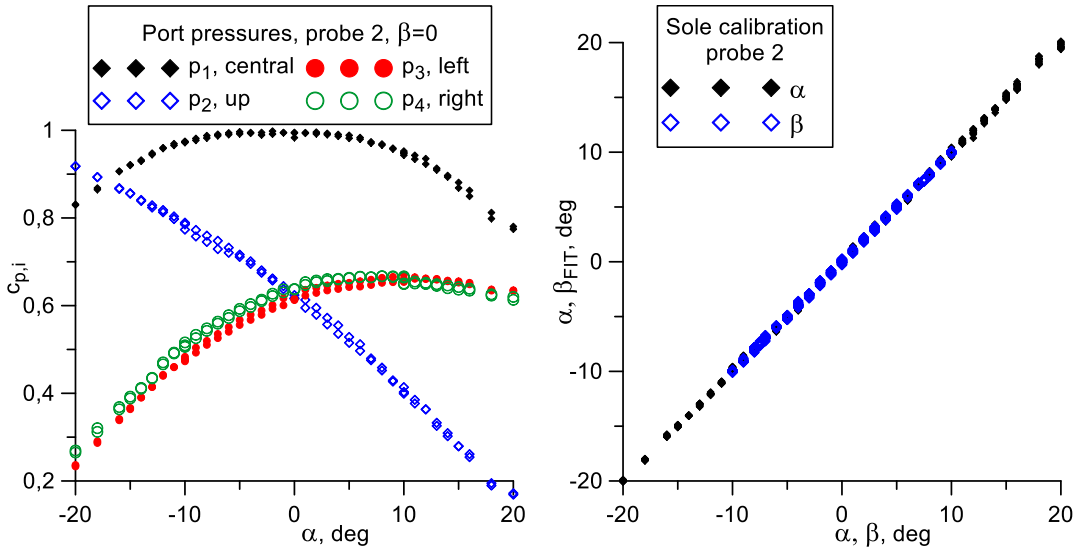

Fig. 8 Pressure coefficients versus α at β=0 (left) results of the fitting functions for α und β (right) of probe 2.

C. In-Situ Calibration within the Flow Field of the UAV

For in-situ calibration, the model was installed in the test section on a strut mounting and traverse system allowing yaw and roll movement, described by the angles θ and φ, respectively (Fig. 3). The combination of these two angles can be transformed into the AoA and AoS via

$$sin\,\alpha = -sin\,\theta\,sin\,\varphi \tag{7}$$

$$sin\,\beta = \frac{sin\,\theta\,cos\,\varphi}{cos\,\alpha} \tag{8}$$

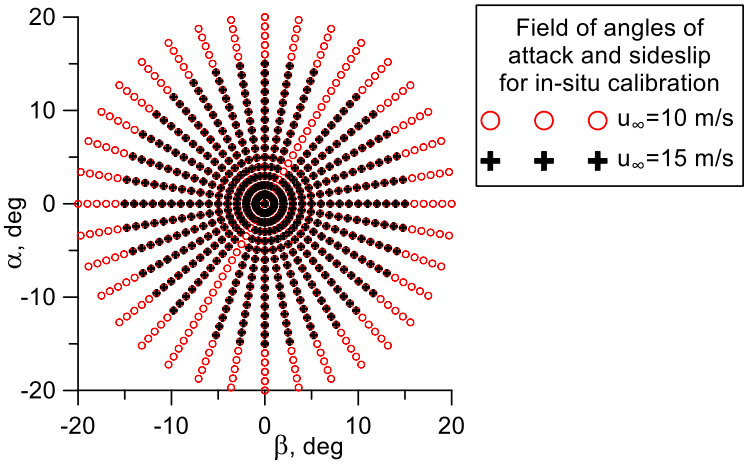

Fig. 9 Field of angles α and β covered by the in-situ calibration.

Fig. 9 shows the field of α-β-combinations resulting from rolling from $\varphi = -90$ deg to $\varphi = +90$ deg and yawing from $\theta = -20$ deg to $\theta = +20$ deg (10 m/s) or from $\theta = -15$ deg to $\theta = +15$ deg (15 m/s), respectively. Note that during the experiment, the rolling angle of $60\,deg$ has been skipped accidentally. The circular structure of the calibration field involves a concentration of small angles α and β, meanwhile combinations of great values of α and β are avoided. This way, outliers that may occur at large flow angles can barely influence the calibration functions. However, including large flow angles into the approximation prevents the polynomial functions from unfavorable behavior caused by extrapolation (cf. Fig. 12 left). Additional tests were conducted to quantify the upstream effects of deflected control surfaces and angular motion.

D. Test Section Blockage

Even though the *UrbanCondor* fits very well into the test section of TU Dresden's wind tunnel, blockage effects cannot be neglected completely. In an open test section, the wind tunnel flow is deflected stronger by the lift of the model than the practically infinite flow field in free flight. This deflection causes additional induced angles of attack that have to be corrected. The correction value is obtained by a lifting line approach based on both model and test section dimensions. This method has been validated by evaluation of the pressure drag of distinct wing models before [14]. Using the lift-slope and zero-lift angle of the *UrbanCondor* determined in AVL, the following relation between geometric angle α and effective angle of attack α_{EFF} which is experienced by the aircraft can be derived:

$$\alpha_{EFF} = 0.924\alpha - 0.837deg \tag{9}$$

V. Results from In-Situ Calibration

The following section shows a number of relevant results achieved with the final set up so far, including comparison with the theoretical prediction. The upstream influence caused by the airframe shows fairly good agreement with the theoretical prediction. This fact allows the correction or calculation of rolling and pitching motion of the whole airframe based on the lifting line model, since experiments to calibrate angular motion did not succeed so far. Only the weak upstream influences originating from control surface deflection have to be estimated from the experimental data.

A. Reynolds-Number Effects

A series of flow velocities ranging from 6 m/s to 19 m/s has been tested for zero angle of attack and sideslip to investigate Reynolds-number dependency. All probe pressures tend to be lower for the smallest velocity as shown in the left diagram of Fig. 10. This value, however, is below the UAV's minimum airspeed, so that this region can be neglected. The input values X and Y for the calibration functions show an even smaller influence of the Reynolds-number, resulting in an angle difference of less than 0.75 deg in AoA and 0.09 deg in AoS for the whole range. Those values are obtained by inserting the Reynolds-dependent variations that are depicted in the right chart of Fig. 10 into the calibration equations (1) - (3). The effect on the reference pressure would result in a difference in calculated flow velocities of up to 5%. Again, these differences occur in a velocity range exceeding the flight envelope of the UAV *Urban Condor*. A more realistic estimation of the deviations to be expected can be drawn from the angular calibration described in the following subsection.

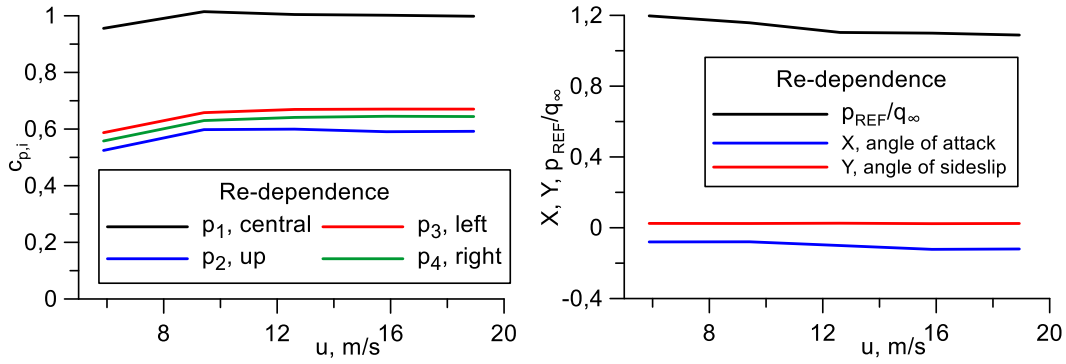

Fig. 10 Reynolds number effects for probe 2 (port side).

B. Angular calibration

Figure 11 shows the recalculated flow angles for the wide calibration range and lower velocity of 10 m/s. Both probes show a fairly good agreement between commanded and recalculated values. Particularly probe 1 shows a certain scattering for large negative angles of attack. For both probes, the sensitivity to side slip angles increases for large AoA values, which is not covered completely by the fitting functions. This is visible in the right chart of Fig. 11 in the AoS range from around -7 deg to $+7$ deg. The points that make the graph appear steeper are those for large AoA values.

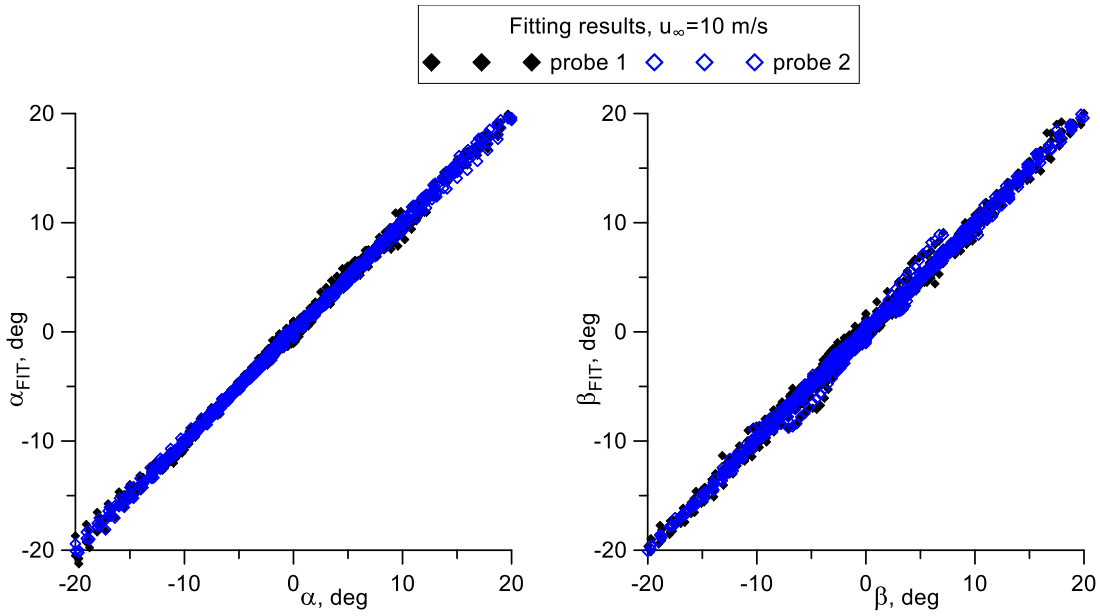

Fig. 11 Fitting results for lower velocity (10 m/s) and greater range of angles (-20 deg to +20 deg). Probe 1 (right wing) is represented by black symbols, probe 2 (left wing) by blue symbols.

For the smaller range of flow angles and higher velocity, the results are similar as shown in Fig. 12. In this case, the data gained from the in-situ calibration have also been evaluated using the sole probe calibration results. This should deliver the actual flow angles within the influence of the airframe. As expected, the upwind field upstream of the wing induces a greater slope, quite similar to what was predicted by the lifting line model. Nonlinearities occur mainly at the onset of positive and negative stall, when the lift and therefore induced flow angles do no longer change linearly with the angle of attack. A more detailed evaluation is presented in subsection C.

As could be expected, the results originating from probe 1 are not reasonable for higher AoA, as shown in the left diagram of Fig. 12. Calibrated only in a range of ±10 deg, the typical behavior of higher order polynomial functions can be observed. This kind of polynomial approach is simply not suitable for extrapolation.

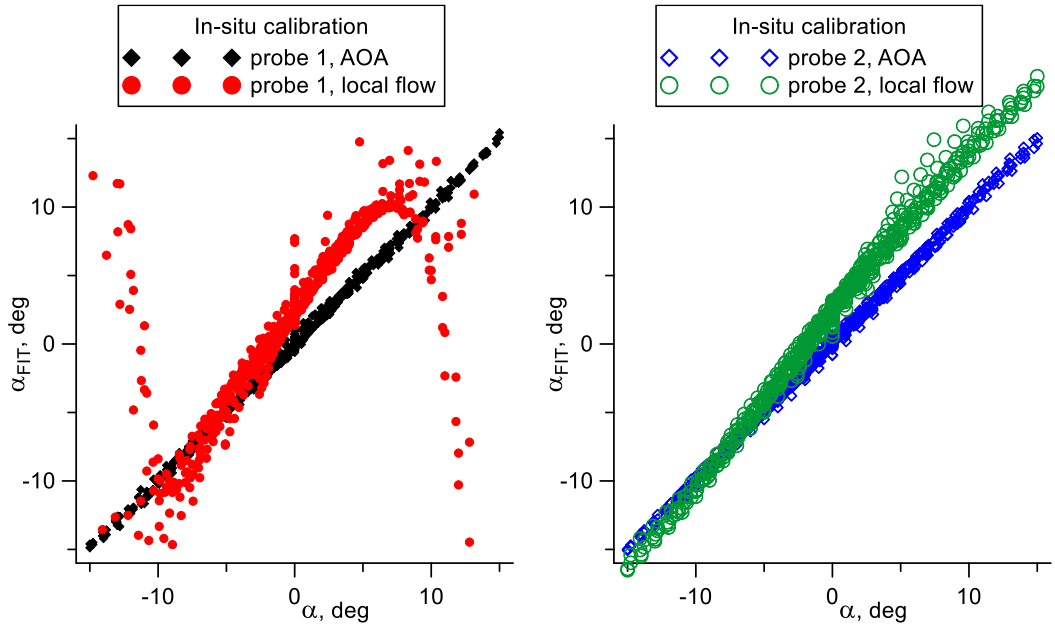

Fig. 12 Recalculated angles of attack and local flow angle probe 1 (left) and probe 2 (right).

Differences between the two angular calibrations, that represent more realistic flight conditions, are smaller than found in the Reynolds-number test, except the sideslip angle. Based on the respective elements of the calibration matrices, the variation ranges from 0.15 deg to 0.34 deg for AoA, from 0.08 deg to 0.28 deg for AoS and from 1.9% to 2% for the dynamic pressure. The resulting uncertainties are considered to be acceptable for the intended purpose of wind estimation.

C. Comparison with Results from the Theoretical Approach

Figure 13 shows the local flow angle detected by probe 2 versus the local flow angle predicted by the theoretical approach presented in section IV A. and B. The black dots symbolize the calculated the flow angle based on the blockage correction (Equ. 9) and the AVL-calculation including 2 deg offset between the probe axis and the aircraft. This is in fairly good agreement with the target line (dashed green). In contrast, the displacement caused by the airfoil thickness is overpredicted by XFOIL. In reality, the displacement can be considered largely neglectable. This insight justifies the effort of calibrating the probes together with the whole aircraft.

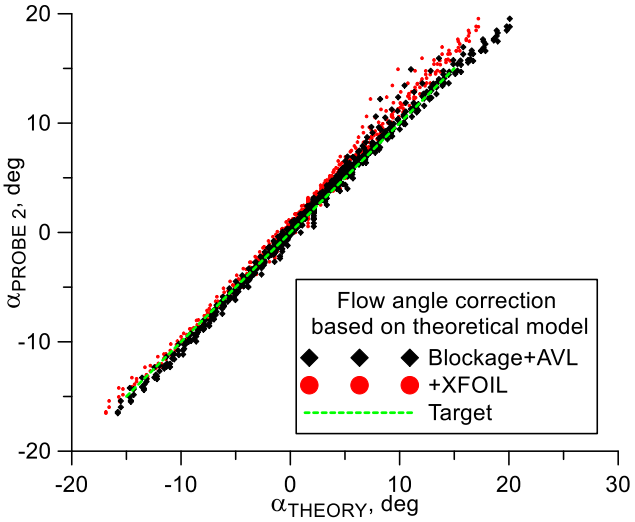

Fig. 13 Local flow angle detected by probe 2 versus local flow angle predicted by blockage correction and vortex lattice model (black dots) as well as displacement caused by airfoil thickness (red dots).

D. Effect of Flap and Aileron Deflection

Within a separate campaign, the upstream effect of deflected control surfaces on the probe positions was examined. Generally, a 2 deg offset was observed compared to the calibration campaign, probably due to a misalignment during reinstallation. This experience shows the importance of a correct definition of the coordinate systems, in particular for the later use in free flight.

The control surface deflections are commanded via the digital control system and are given in so called PWM values. The connection to actual angles could not be characterized before the wing has been destroyed during one of the consecutive test campaigns. Using 3D-printing technology, the new wing will be identical and this characterization can be made up leeway. From the characterization of the elevator, a ΔPWM of 1000 corresponds with a control surface deflection of 60 deg. In operation however, the most valuable information is to know the difference in measured flow angle depending on the control command.

The measured effect remains within the noise level, but can clearly be extracted from the averaged values (shown in Fig. 14).

AVL predicts a change of 0.8 deg in local flow angle due to 30 deg of aileron deflection, the linear fit yields -0.38 deg and 0.27 deg (starboard/portside) for a ΔPWM of 500 (equal to 30 deg). For 30 deg of flap deflection the predicted change in local flow angle is 2.17 deg, meanwhile the averaged measured values show only 0.6 deg for full flaps.

These differences are in the range that is to be expected for the effectiveness of a flap for the given Reynolds number ($3.3 \cdot 10^5$ at 10 m/s) compared to an inviscid flow, which is assumed in lifting line calculation. Figure 15 gives an impression of the impact on flap effectiveness caused by viscid flow.

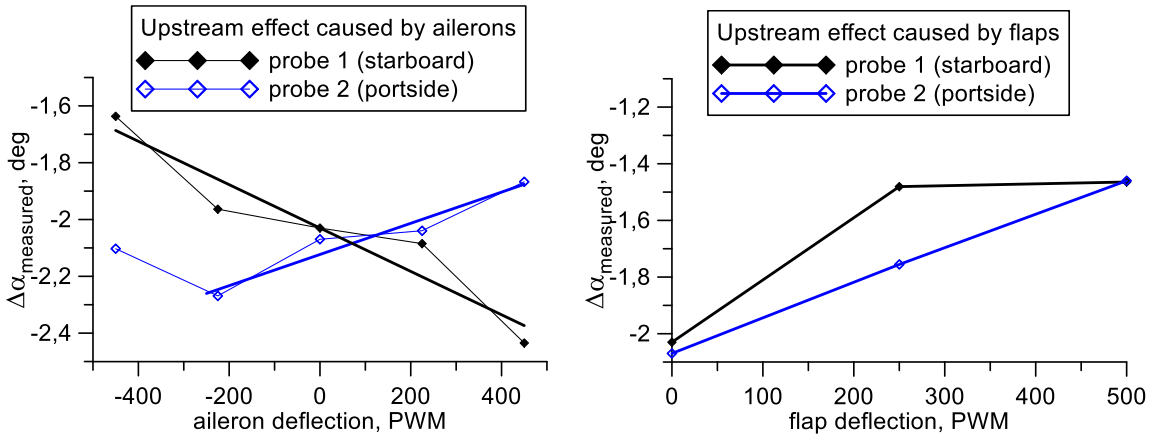

Fig. 14 Upstream effect of deflected control surfaces on the angle of attack detected by the probes, left: ailerons, right: flaps.

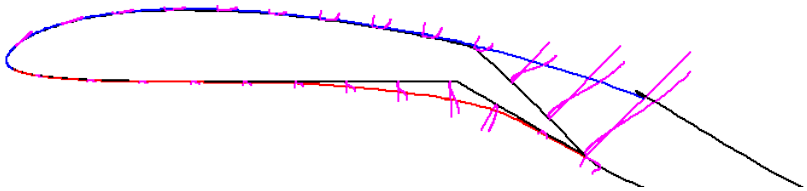

Fig. 15 XFOIL calculation of the flow over a Clark-Y airfoil with a 30-deg flap at α=0, Re=3.3·10^5; the lift increase compared to the clean airfoil is only $\Delta c_{L,visc}$=0.96 against $\Delta c_{L,invisc}$=2.16 for the inviscid case.

VI. Conclusion

The presented investigations prove that four-hole probes with continuous calibration function can cover a sufficient range of flow angles for flight attitude measurements on UAVs. They require a minimum of system resources concerning probe size, pressure transducers, A/D-channels and onboard computing power. Flow angle probes can be calibrated together with UAVs in medium-sized wind tunnels. Blockage correction still remains necessary. Traverse systems that produce angles of attack and sideslip by superposition of yawing and rolling angle provide a favorable distribution of AoA and AoS for probe calibration. Lifting line models are capable to predict upstream influence of the entire airframe onto the probe position and should also be trusted to calculate additional local flow angles caused by angular motions of the aircraft. However, the upstream effect of control surfaces is largely overpredicted by lifting line models, since the effectiveness of control surface deflection itself is strongly depending on viscous flow properties. Based on previous experiences from free flight experiments (Fig. 5), appropriate filtering is necessary to obtain reasonable wind data.

Acknowledgments

This research was funded by the German Federal Ministry for Digital and Transport under grant number 19F1176A. The responsibility for the content of this paper is with its authors. The financial support is gratefully acknowledged.

References

[1] Rienecker, H., Hildebrand, V., and Pfifer, H., “Energy Optimal Flight Path Planning for Unmanned Aerial Vehicles in Urban Environments Based on a Novel Energy-Distance Map,” SciTech, 2024.

[2] Frey, J., Schubert, S., Rienecker, H., Hildebrand, V., and Pfifer, H., “Wind Tunnel Measurement of the Urban Wind Field for Flight Path Planning of Unmanned Aerial Vehicles," SciTech, 2024.

[3] Xiang, X., Wang, Z., Mo, Z., Chen, G., Pham, K., and Blasch, E., "Wind field estimation through autonomous quadcopter avionics," 2016 IEEE/AIAA 35th Digital Avionics Systems Conference (DASC), Sacramento, CA, USA, 2016, doi: 10.1109/DASC.2016.7778071.

[4] Prudden, S., Fisher, A., and Mohamed, A., Watkins, S., "An anemometer for UAS-based atmospheric wind measurements," 17th Australian Aerospace Congress, 26-28 February 2017, Melbourne.

[5] Pu, O., Yuan, B., Li, Z., Bao, T., Chen, Z., Yang, L., Qin, H., Li, Z., "Research on the Characteristics of Urban Building Cluster Wind Field Based on UAV Wind Measurement," Buildings 2023, 13, 3109. https://doi.org/10.3390/buildings13123109.
[6] Treaster, A. L., and Yocum, A. M., “The calibration and application of five-hole probes,” 24th International Instrumentation Symposium, 1978, pp. 255–266.
[7] Zilliac, G.G., "Modelling, calibration, and error analysis of seven-hole pressure probes," In: Experiments in Fluids, vol 14., pp. 104-120, 1993.
[8] Shepherd, I. C., “A Four Hole Pressure Probe for Fluid Flow Measurements in Three Dimensions,” J. Fluids Eng., vol. 103, no. December, pp. 590–594, 1981. https://doi.org/10.1115/1.3241774.
[9] http://turbulentflow.com.au/Products/CobraProbe/CobraProbe.php, retrieved 13th May, 2024.
[10] Frey, J., "Strömungsmessung im Freiflug," idaflieg-Berichtsheft Nr. 34, 2009, pp.27-41.
[11] https://sigmfg.com/products/sig-kadet-lt-40-egv-arf, retrieved 13th May, 2024.
[12] Drela, M., Youngren, H.: “MIT AVL User Primer – AVL 3.36," 2017.
[13] Drela, M.: "XFOIL: An Analysis and Design System for Low Reynolds Number Airfoils," In: Mueller, T.J. (eds) Low Reynolds Number Aerodynamics. Lecture Notes in Engineering, vol 54., pp. 1-12, 1989.
[14] Frey, J., Sell, F., Gillespy, R., Pfifer, H., "Aerodynamic Design and Wind Tunnel Test of a Laminar Wing with Split Flap for a Fuel Cell Powered Aircraft," DLRK 2022, https://doi.org/10.25967/570209.